



# OpenMesh: Wireless Signal Dataset for Opportunistic Urban Weather Sensing in New York City

Dror Jacoby<sup>1</sup>, Shuyue Yu<sup>2</sup>, Qianfei Hu<sup>2</sup>, Zachary Hine<sup>2</sup>, Rob Johnson<sup>5</sup>, Jonatan Ostrometzky<sup>1</sup>, Igor Kadota<sup>3</sup>, Gil Zussman<sup>4</sup>, and Hagit Messer<sup>1</sup>

<sup>1</sup>School of Electrical Engineering, Tel Aviv University, Tel Aviv, Israel

<sup>2</sup>Department of Computer Science, Columbia University, New York, NY, USA

<sup>3</sup>Department of Electrical and Computer Engineering, Northwestern University, Evanston, IL, USA

<sup>4</sup>Department of Electrical Engineering, Columbia University, New York, NY, USA

<sup>5</sup>NYC Mesh, New York, NY, USA

**Correspondence:** Dror Jacoby (drorjacoby@mail.tau.ac.il)

**Abstract.** We introduce OpenMesh, a publicly available dataset of wireless signal measurements from a community-run communication network in New York City. While originally designed for affordable internet access, these links can be used opportunistically for high-resolution weather monitoring in dense urban areas, providing 1-minute sampling and dense spatial coverage. Spanning eight months of measurements (November 2023 to June 2024), the dataset comprises 103 directional links in Lower Manhattan and Brooklyn, operating in three primary frequency ranges: 5–6 GHz (C-band), 24 GHz (K-band), and 58–70 GHz (V-band)—part of the millimeter-wave (mmWave) spectrum.

Our analysis incorporates meteorological records from the study period, including precipitation from local weather stations, thereby enabling real-time analysis of signal-weather relationships and expanding in-city applications through opportunistic sensor networks. During the study period, diverse weather events—ranging from intense rainfall that caused link attenuations of up to 30 dB and occasional outages, to snowstorms in Winter 2024—demonstrated the network’s potential for broader meteorological sensing. Analyzing multi-band observations provides valuable insights into emerging 5G/6G challenges and uncovers new opportunities for urban environmental monitoring. The OpenMesh dataset is available at <https://doi.org/10.5281/zenodo.15268340> (Jacoboy et al., 2025). By publishing both the datasets and our preliminary analyses, we hope to encourage further research that leverages wireless networks in dense urban areas for real-time sensing.

## 1 Introduction

Opportunistic sensing (OS) uses a variety of non-traditional sensors—such as personal weather stations (PWS), commercial microwave links (CMLs), and satellites—to support environmental monitoring. Accurate meteorological observations, including precipitation monitoring, are essential in fields ranging from water management and agriculture to urban planning, flood control, and risk management (Bojinski et al., 2023; Ravuri et al., 2021). Although traditional weather measurements, such as weather radars and rain gauges (RGs), can provide broad-scale coverage, they often require costly infrastructure. Radars, in particular, suffer from clutter, path attenuation, and interference, and frequently require further calibration (Zawadzki, 1984).



Rain gauges, while considered accurate, provide only point measurements, often lack spatial detail, and can be scarce in many regions (Hu et al., 2019).

Therefore, opportunistic data streams, such as those from OS networks, can offer detailed local insights that are crucial for capturing urban microclimatic variations, with dense deployments providing complementary or even alternative coverage to traditional observations. By repurposing infrastructure not built for meteorological purposes—particularly communication systems—OS enables efficient collection of environmental data with fine temporal and spatial resolution. Furthermore, with the recent development of AI techniques that have transformed weather forecasting—from minute-scale nowcasting to longer-range horizons (Bi et al., 2023; Conti, 2024). —through the capture of complex patterns from extensive, diverse datasets and the leveraging of big-data analytics, OS networks can significantly enhance spatiotemporal resolution and data diversity, ultimately benefiting scientists and decision-makers.

Wireless networks operating in microwave (1-30 GHz) and mmWave 30-300 GHz) bands exemplify OS technology. While mmWave frequencies deliver high data throughput, they are also highly susceptible to atmospheric conditions and blockages (ITU-R P.838, 2005; Niu et al., 2015), resulting in severe attenuation during precipitation events. By leveraging this inherent sensitivity, OS approaches transform what would otherwise be a “source of error” into a cost-efficient meteorological signal, effectively repurposing existing communication infrastructure for environmental sensing (Messer et al., 2006).

As beyond-5G (B5/6G) networks evolve to employ higher-frequency links in dense, small-cell architectures, they create novel opportunities for real-time environmental sensing (Seker et al., 2018; Niu et al., 2015; Janco et al., 2023; Santos, 2018; Castello et al., 2021). This progression naturally leads to Integrated Sensing and Communication (ISAC), where communication infrastructure is designed for both data transport and environmental sensing under unified framework (Xu et al., 2023; Cui et al., 2023; Dong et al., 2022; Kaushik et al., 2024).

A growing number of open data efforts (Fencl et al., 2023, 2025) – including *OpenMRG* in Sweden (Andersson et al., 2022), a country-wide dataset in the Netherlands (Overeem, 2023), and *OpenRainER* in Italy (Action, 2023) – show how CML data can fill observational gaps. These initiatives highlight the potential of OS to extend research in diverse climates and network topologies. Here, we introduce a publicly available dataset covering a newly monitored sector of New York City (NYC)—comprising multi-band wireless link measurements gathered from the rapidly expanding NYC Mesh community network in its dense urban environment. The OpenMesh dataset pairs minute-scale microwave and mmWave measurements across multiple bands (~5, 24, 60, 70 GHz) with link lengths ranging from tens of metres to several kilometres, creating a uniquely rich test-bed for investigating the role of next-generation networks (NGNs) in city-scale wireless-sensing applications. In our analysis, we assess these sensing capability of the OpenMesh dataset by comparing with co-temporal meteorological records from opportunistic and standard weather stations (WS) across the study period. Fine-grained analysis of rainfall and snow events shows close alignment between the link signals and reference observations, demonstrating these wireless networks’ potential as opportunistic urban weather sensors for real-time applications. By publicly sharing the OpenMesh dataset and demonstrating its applicability, we expand OS resources and illustrate how emerging wireless networks can act as opportunistic environmental sensors in densely sampled urban settings.

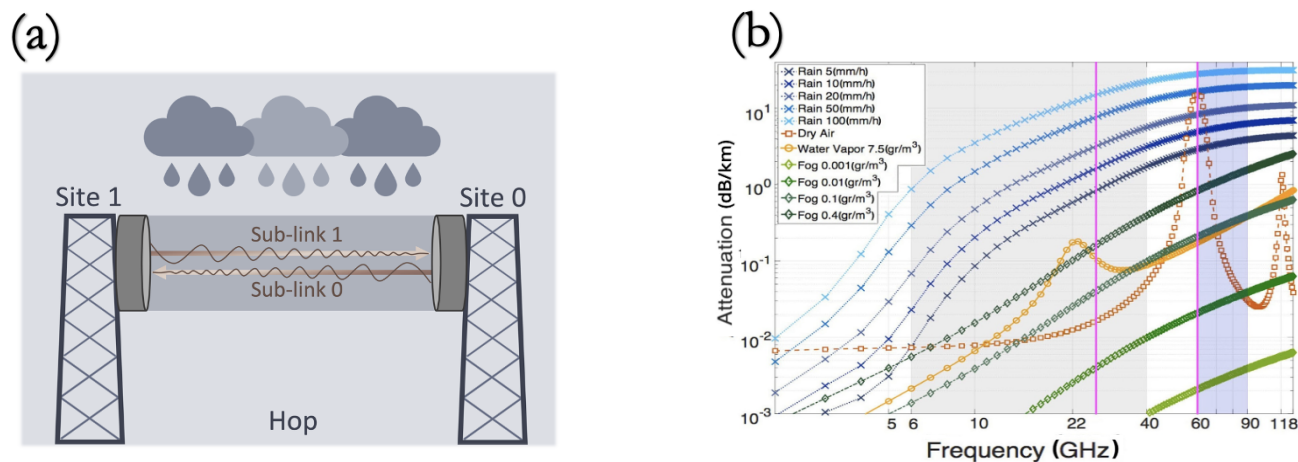


**Figure 1.** (a) Schematic of a point-to-point wireless communication link (Fencl et al., 2023). (b) Signal attenuation per km for various atmospheric phenomena as a function of frequency (ITU-R P.530, 2017; Ostrometzky, 2017).

**Organization of This Paper.** Sect. 2 outlines the dataset’s features and unique characteristics. Sect. 3 examines wireless link performance under precipitation, and Sect. 4 demonstrates rain detection and high-resolution mapping. Sect. 5 discusses challenges, opportunities, and future directions, while Sect. 6 details data availability, and Sect. 8 provides concluding remarks.

## 2 Dataset Overview

60 This section introduces the dataset, outlining its collection process and background for environmental monitoring. It focuses on two forms of OS data in NYC: (i) OpenMesh—published wireless-link data from NYC Mesh, and (ii) meteorological records, which we use for validation and comparison.

### 2.1 Wireless Links

#### 2.1.1 Microwave & mmWave Links

65 Wireless communication links are point-to-point (P2P) radio connections between two fixed locations. Wireless communication links, often employed by mobile and enterprise networks for backhaul, are also widely used in smart-city applications and community-driven projects (e.g., NYC Mesh), offering both commercial and public connectivity. Depending on the frequency and application, these links can span from a few meters to several kilometers and are commonly employed for backhauling, building-to-building data transfers, and other network services. Network Management Systems (NMS) typically collect link  
70 performance data to automate network monitoring and quality management, but storing or archiving these datasets is not always mandated and often depends on specific network standards and operator practices.



The following describes the structure of wireless link elements (Fencl et al., 2023): A ‘site‘ is defined as the physical location hosting one or more antennas, while a ‘sublink‘ refers to a one-directional path between antennas. A ‘link‘ comprises all ‘sublinks‘ connecting two antennas, and a hop encompasses every link connecting two sites, as shown in Fig. 1a. Both microwave (1–30 GHz) and mmWave (30–300 GHz) systems are crucial for x-haul (fronthaul, midhaul, and backhaul), connecting access nodes to core networks for data transmission. Wireless measurements can originate from diverse providers, including cellular telecommunication companies, municipal smart-city operators, and community-driven networks like the one presented here. Each features distinct topologies and coverage densities. In NGNs—including smart-city infrastructures—antennas operate across a wide frequency range, from sub-6 GHz to high mmWave bands, enabling flexible, short-range deployments. By strategically using diverse frequency bands, these systems adapt to varied applications in complex urban environments. Small cells are typically mounted on rooftops, utility poles, or other urban fixtures, delivering localized high-throughput connectivity at distances ranging from a few meters to multiple kilometers. These deployments seamlessly integrate with the existing digital infrastructure, expanding capacity and enhancing key features like mobility and low latency—particularly crucial in dense urban environments.

**Signal Level Measurements.** Wireless networks typically measure signals strength using two key metrics: the transmitted signal level (TSL) and the received signal level (RSL), both expressed in dBm. The difference between them, referred to as total attenuation (in dB), is given by

$$A_{\text{tot}}(t) = TSL(t) - RSL(t). \quad (1)$$

Depending on the operator’s protocols, TSL and RSL are often logged at intervals ranging from seconds to minutes, hours, or even days, stored either as instantaneous values or aggregated statistics (e.g., mean, minimum, or maximum) for each sampling window. In addition, these network protocols typically quantize measurements which affects data precision. Together, these factors ultimately define the dataset’s resolution and precision. The total attenuation,  $A_{\text{tot}}(t)$ , arises from multiple factors such as free-space path loss; scattering, reflection, and diffraction by obstacles (e.g., buildings or terrain) further affect the signal. Additionally, atmospheric conditions (e.g., humidity, temperature inversions, and gaseous absorption) can compound these losses. When precipitation is present, raindrops or snowflakes introduce an extra attenuation term along the path (ITU-R P.838, 2005). In Fig. 1b, the influence of several atmospheric phenomena on the expected attenuation (in  $\text{dBkm}^{-1}$ ) is illustrated. A pronounced absorption peak occurs near 60 GHz due to oxygen resonance (Arvas and Alsunaidi, 2019), while rainfall increasingly dominates overall attenuation at most frequencies—especially at higher bands, which suffer from increased rain-induced attenuation.

**Environmental Monitoring with Wireless Links.** The power measurements collected from existing communication links can effectively function as environmental sensors (Messer et al., 2006), leveraging their sensitivity to atmospheric phenomena such as rain in an opportunistic approach. Therefore, they can form part of wireless sensor networks for urban precipitation monitoring (Upton et al., 2005; Overeem et al., 2011). Indeed, a variety of efforts worldwide have harnessed wireless link data for environmental monitoring applications—especially precipitation (Graf et al., 2020; Messer and Gazit, 2016; Overeem, 2023; Chwala and Kunstmann, 2019; Zhang et al., 2023; Špačková et al., 2021)—by utilizing the attenuation caused by rainfall



**Table 1.** Dataset Overview: NYC Mesh Sublinks by Frequency and Weather Stations

Data Source	Count (Sublinks/Stations)	Temporal Resolution	Measured Variable	Resolution
Mesh Wireless Links	5 GHz (5.0–6.0 GHz): 54	1 min	RSL	1 dBm
	24 GHz (24.0–24.5 GHz): 8			
	60 GHz (58.0–66.0 GHz): 25			
	70 GHz (66.0–69.5 GHz): 15			
	<b>Total: 103</b> <sup>(a)</sup>			
<i><sup>(a)</sup> Among these, links use multi-band with two frequencies (60/70 GHz + 5 GHz backup) to mitigate rain fade.</i>				
<b>Weather Dataset</b>				
WUnderground Regular PWS	45	5 min	Precip. Rates <sup>(b)</sup>	0.25 mm
WUnderground Airports	2	30 min	Precip. Rates, Condition <sup>(b)</sup>	0.25 mm
NOAA	3	Daily	Accum. Precip. & Snowfall	0.25 mm
<i><sup>(b)</sup> Weather Station data also include additional meteorological variables.</i>				

along the radio path. Beyond rain, wireless communication sensing methods have expanded exploring meteorological variables such as humidity, fog, wind, and even air quality (Messer et al., 2012; Rubin et al., 2022; David et al., 2014). With the rapid development of NGN architectures (B5G/6G) planned for dense urban environments—enabling high temporal and spatial resolutions and unlocking new opportunities and challenges for urban environmental sensing (Ostrometzky and Messer, 2024; Janco et al., 2023; Zhang, 2023)—the potential usage of communication networks is expanding toward in-city dense wireless sensor networks.

The variety of OS dataset sources and methods—including wireless links—has prompted global initiatives to establish a unified reference community and standards. One such effort is the Global Microwave Link Data Collection Initiative (GMDI) (Fencel et al., 2025), which aims to foster collaboration among scientists, national weather services, sensor-network owners, and end-users of hydrological products.

### 2.1.2 NYC Mesh Network

NYC Mesh is a volunteer-led, community-driven network that provides affordable, high-speed internet across NYC (Mesh, 2025.). By deploying rooftop nodes and using a decentralized mesh infrastructure, it reduces reliance on traditional internet service providers while promoting digital equity—without logging personal data or censoring content, thus preserving privacy and neutrality. Coverage is currently concentrated in Brooklyn and Lower Manhattan, with ongoing expansion into the Upper West Side, Harlem, and the Bronx. With volunteer-built broadband networks demonstrate how existing urban infrastructure can offer a low-cost alternative to traditional, centralized Internet Service Providers (ISPs). Mesh architectures dynamically assign traffic, maintaining robustness if a node or link fails—particularly in dense urban settings—and often record real-time performance metrics for coverage and service quality. Nodes, acting as both transmitters and receivers, form a fault-tolerant web by routing data through multiple paths.

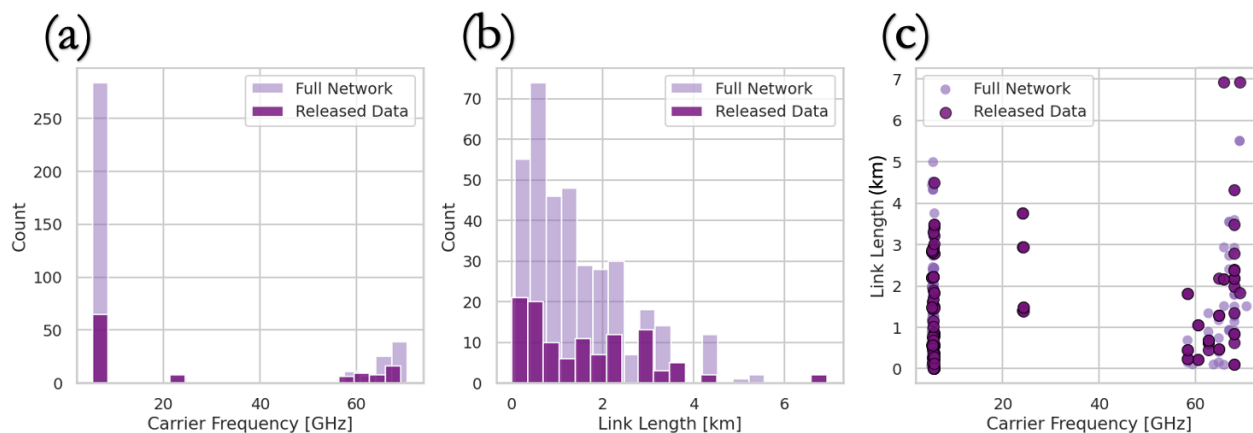


**Figure 2.** Feature distributions of OpenMesh dataset: sublink lengths range in kilometers (km) and carrier frequencies (GHz).

Recent work on community cellular networks highlights how coverage visualizers reduce volunteer workload, improve network reliability, and identify potential failures (Kittivorawong et al., 2024). In addition to operating public Wi-Fi hotspots, NYC Mesh maintains an open <https://wiki.nycmesh.net/> (*Wiki*) and a <https://github.com/nycmeshnet/nycmesh.net> (*GitHub repository*), enabling collaborative updates and service enhancements.

130 **Mesh Networking Configuration.** Mesh networking is a decentralized model in which every node cooperatively forwards data, forming a multi-hop network that doesn't depend on any single device or connection to stay online. In urban settings, routers mounted on rooftops or street poles create an interconnected coverage area that can replace or augment the usual "last mile" provided by hierarchical, wired ISPs, thus bypassing many complexities associated with traditional centralized infrastructures. NYC Mesh exemplifies this approach by leveraging diverse wireless hardware and protocols to deliver reliable  
135 broadband connectivity across NYC. NYC Mesh employs a tiered network architecture that combines mesh principles with a hub-and-spoke design: (i) *Supernodes* are high-capacity sites, typically housed in data centers or high-rise locations and equipped with fiber uplinks serving as primary Internet gateways; (ii) *Hub Nodes* are neighborhood-level relay points that aggregate traffic from rooftop installations and forward it either to other hub nodes or directly to supernodes. and (iii) *Member Nodes* are rooftop or building installations that connect to either a hub or supernode, forming a multi-layered web of links. This  
140 tiered arrangement enables extensive coverage and maintains resiliency through multiple redundant paths—if one node or link fails, traffic is dynamically rerouted to ensure uninterrupted service.

**Network Hardware and Spectrum** NYC Mesh employs cost-effective hardware from vendors such as Ubiquiti and MikroTik to build a resilient urban network. Devices like Ubiquiti LiteBeam AC, NanoStation, and MikroTik LHG are selected based on link distance and frequency requirements, and multiple hub-to-supernode loops dynamically redirect traffic and eliminate single  
145 points of failure. Wireless links are strategically deployed to exploit multiple frequency bands to balance speed, range, and resilience across its urban network. In the 5 GHz band, devices such as Ubiquiti's LiteBeam and airFiber 5XHD deliver typical



throughput of 75–300 Mbps over distances of up to 3–5 km in point-to-point or multipoint configurations, suited for the bulk of outdoor links. For higher-capacity, shorter-range connections, the 24 GHz band (e.g., via airFiber 24) offers around 750 Mbps over links reaching up to 5 km. When even greater bandwidth is required for backbone connectivity, the 60 GHz band is used—with equipment like Ubiquiti’s airFiber 60 LR/XR and Mikrotik’s LHG 60 achieving high bandwidths, though typically limited to 500 m–3.5 km due to higher attenuation. Additionally, licensed spectrum in the 70–80 GHz range—employed by systems such as the Siklu Etherhaul Kilo—supports ultra-high capacities up to 10 Gbps. However, in dense urban environments, these manufacturer-specified ranges are typically reduced by approximately 50%. For further details on network hardware and equipment, see (Mesh, 2025.).

**155 Data Collection Pipeline** Wireless link metrics are collected through NYC Mesh’s Zabbix monitoring system, which archives Simple Network Management Protocol (SNMP) statistics from Open Shortest Path First (OSPF)–discovered devices, together with telemetry pulled via the UISP API. These feeds supply 1-minute measurements that form the backbone of the OpenMesh dataset. The OSPF data API, maintained by NYC Mesh, is reachable from any node within the mesh’s private IP space; each device’s JSON payload is refreshed every minute, with an updated timestamp confirming freshness. We establish a fully automated pipeline runs daily: it queries the NYC Mesh inventory for active devices, fetches 1-minute time-series of link metrics— such as signal strength(dBm), capacity(Mbs<sup>-1</sup>), latency (ms), and throughput (Mbs<sup>-1</sup>)—and performs standard reliability checks, retrying any failed or incomplete requests before uploading the validated records to a cloud database for long-term analysis. The metrics collected describe link’s quality only, do not contain user-level information, and the pipeline can be reconfigured for higher temporal resolutions to support real-time sensing and network management applications.

### 165 2.1.3 Case Study

The OpenMesh dataset spans eight months (2023-10-29 to 2024-07-01), with all timestamps recorded in UTC. The dataset comprises two main components:

1. **Raw measurements:** Time-series data spanning the entire study period.
2. **Metadata:** Tables describing each sensor’s fixed attributes (e.g., physical location, carrier frequency, link length, etc).

170 The OpenMesh dataset is a curated subset of the broader NYC Mesh network, which comprises several hundred wireless links and is still expanding. Table 1 summarizes the OpenMesh sub-link characteristics. The archive provides open-access RSL measurements (dBm) for 103 sub-links, sampled once per minute with 1 dBm resolution and vertical polarization. Fig. 2 plots the carrier frequencies and path lengths (transmitter–receiver distances) of these sub-links alongside other active NYC Mesh devices instrumented for data collection. The 103 sub-links were selected for continuous data availability during the study window and to span a broad range of frequencies and path lengths, enabling detailed analysis of how atmospheric phenomena influence various network features in a dense urban setting.

Missing data appear as gaps caused by link outages, which can arise from hardware failures, collapses, or severe weather-induced attenuation. Two notable missing raw data gaps are specified: (i) *Late startup*: A subset of around 30% sublinks began data collection on 7 November, leaving an initial gap of over one week after the nominal start date. (ii) *Hardware Outage*:

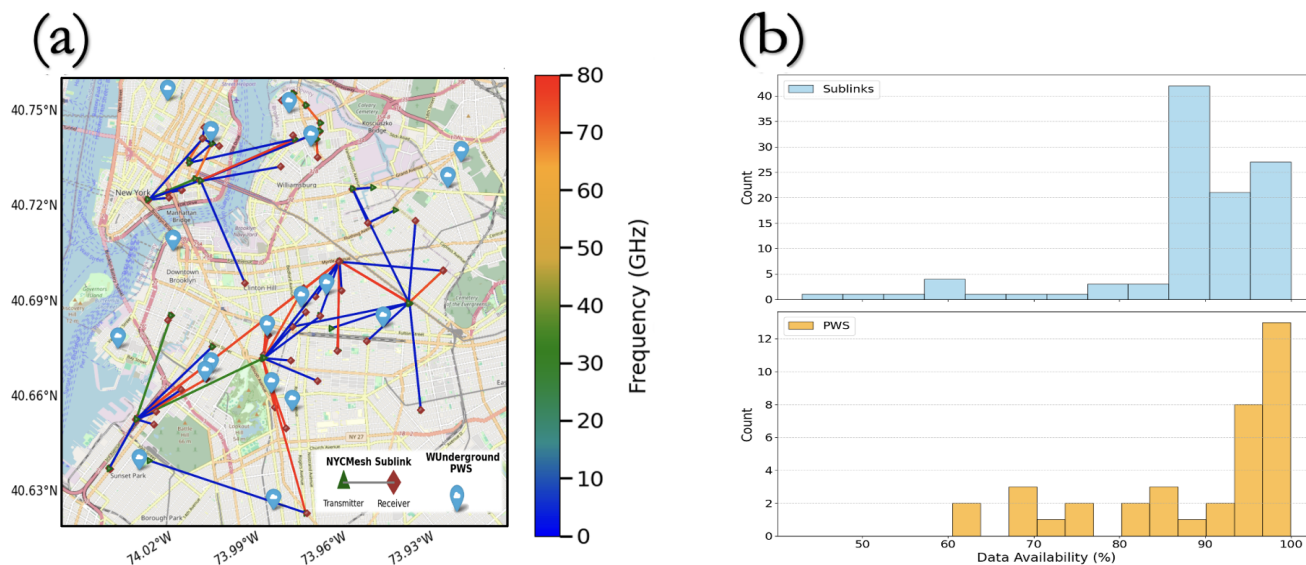


**Figure 3.** (a) OpenMesh sublinks in Brooklyn area coloured by operating frequency (5–70 GHz), with nearby PWS locations. © Open-StreetMap contributors 2025. Distributed under the Open Data Commons Open Database License (ODbL) v1.0. (b) Data-availability histograms for NYC-Mesh sublinks (top) and WUnderground PWS (bottom). The x-axis shows the percentage of the total measurement period each sensor was active, and the y-axis the number of sensors in each availability bin.

180 During the first week of March, a network-collection hardware failure for roughly one week, resulting in missing or corrupted data samples.

## 2.2 Meteorological Data

To evaluate our wireless-based observations, we collect meteorological data from NYC, summarized in Table 1. WS record meteorological variables in a specific location using dedicated sensors such as thermometers (temperature), barometers (pres-  
185 sure), anemometers (wind), and gauges for precipitation. Official WS often follow standardized protocols and guidelines from organizations like the World Meteorological Organization (WMO), ensuring consistency and comparability across station networks. As a result, they serve as reliable references for validating or calibrating other observational systems. However, even well-maintained official stations typically provide only limited spatial coverage—underscoring the need for supplementary data sources in dense urban environments.

### 190 2.2.1 PWS: Personal Weather Stations

PWS are deployed by individuals or local organizations to collect localized meteorological data in near real-time. They can fill observational gaps, particularly in dense urban neighborhoods where official coverage might be limited. PWS have become increasingly popular for collecting rainfall data, but their quality can vary greatly—common problems include faulty zeros,



missing data, and bias—often stemming from improper setups. Therefore, quality control methods can help address these  
195 issues El Hachem et al. (2024), underscoring the need for further evaluation under diverse conditions. Following recommended  
calibration routines and standardized sensor placement can substantially enhance PWS data quality (El Hachem et al., 2023).  
Although variations in sensor quality, calibration, and maintenance practices can affect PWS data reliability, their high spatial  
density and responsiveness make them valuable for fine-grained weather analysis.

**Weather Underground (WUnderground).** WUnderground<sup>1</sup> leverages an extensive global PWS network, currently exceed-  
200 ing 250,000 stations, with more than 180,000 located in the United States. This online platform collects and shares real-  
time weather observations, forecasts, and historical records. WUnderground integrates localized data with advanced forecast-  
ing models, enabling high-resolution analyses of microclimates, precipitation trends, and other atmospheric phenomena. The  
present study uses this resource to obtain time-stamped weather records aligned with network performance metrics, thus allow-  
ing a detailed examination of how meteorological conditions influence wireless signals. Although precipitation is our primary  
205 focus, the WUnderground records also include additional meteorological variables—such as temperature, wind speed and di-  
rection, humidity, air pressure, solar irradiance, and dew point—that could be leveraged in future works, extending research  
opportunities and applications of OpenMesh dataset.

**Precipitation Collection.** To measure precipitation, the WUnderground station uses a self-emptying tipping bucket design with  
a collector area of 20mm, capturing rainfall in increments of 0.25mm and employing protective meshes to block contamination.  
210 Standard, unheated PWS devices often fail to differentiate precipitation types, might lead to delayed or underreported data for  
non-liquid forms (snow, hail, etc.). As a result, snow or frozen-precipitation measurements may be incomplete or imprecise.  
We highlight these constraints in our study and emphasize the need for additional data validation when analyzing precipitation-  
driven processes.

### 2.2.2 Precipitation Measurements

215 This study primarily focuses on precipitation data, combining observations from standard WS and PWS across NYC. We  
leverage meteorological data from two main sources: WUnderground, offering a dense PWS network with broad spatial cov-  
erage and high sampling rates, and the National Oceanic and Atmospheric Administration (NOAA), which provides officially  
validated measurements. We categorize three types of sensors:

- **Standard PWS (WUnderground)** Data from a total of 45 PWS distributed across Brooklyn and Manhattan provide  
220 detailed meteorological variables—including precipitation—at 5- to 15-minute intervals. These stations are part of a  
continuously growing PWS network with near real-time updates and quality controls. This high temporal resolution and  
spatial coverage enable comprehensive analyses of short-term weather patterns in the area, supporting evaluations of  
potential local impacts on communication links.
- **Airport WS (WUnderground).** Hourly observations from John F. Kennedy (JFK) and LaGuardia (LGA) airports in-  
225 clude aviation-relevant parameters (e.g., fog, precipitation type), thereby offering insight into mixed-weather events and

<sup>1</sup><https://www.wunderground.com>

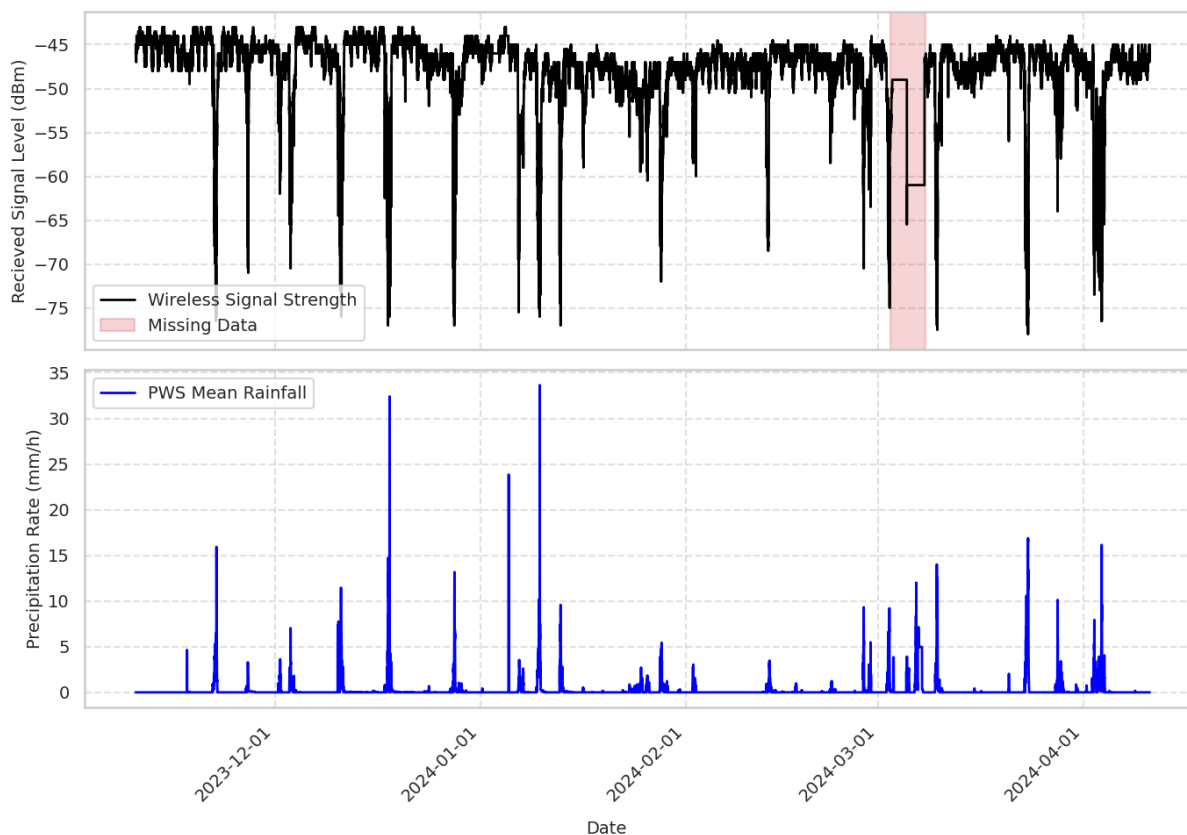


**Figure 4.** Data measurement demonstration: Wireless signal and precipitation data over time, with RSL measurements (dBm) of a 69 GHz NYC Mesh link alongside the mean precipitation rate ( $\text{mm h}^{-1}$ ) recorded by a nearby PWS throughout a five-month study period.

contributing to broader conditions across the region. These measurements, derived from the standardized Automated Surface Observing Systems (ASOS) network, provide consistent and calibrated data essential for safe air traffic management and serve studies as a reliable benchmark, with also more comprehensive details.

- **NOAA Stations.** Historical daily summaries from JFK, LGA, and Central Park (CP) are obtained through NOAA. These official ASOS records distinguish between new snowfall (i.e., what fell in the previous 24 hours) and the total snow depth on the ground, while also providing rainfall accumulation. NOAA serve as a trusted baseline against which other datasets can be cross-checked for precipitation verification. providing an established baseline against which other datasets can be cross-checked to verify precipitation.

230



## 2.3 Dataset Characteristics

235 The OS dataset merges attenuation measurements from OpenMesh sublinks with meteorological observations from nearby  
PWSs, enabling real-time, high-resolution spatio-temporal analysis and alignment from both sources. Fig. 3a maps the OS  
subset in Upper Brooklyn: sublinks (colour-coded by carrier frequency) and PWS sites form a dense network spanning roughly  
10 km × 10 km. While this figure illustrates the OpenMesh data in Brooklyn area, the wider NYC Mesh network contains larger,  
denser network—including links in Lower Manhattan and Harlem—outlined in Fig. 2. For the present study we focus on this  
240 representative subset. Fig. 3b provides a histogram of OS data availability after preprocessing steps, showing the percentage  
of valid records relative to the total possible measurements. Missing sensor values are marked with NaNs in our dataset. In  
practice, most published sublinks achieved around 90 % availability, ensuring robust coverage over the study period.

To prepare these heterogeneous sources for analysis over the study period, we applied a series of preprocessing steps includ-  
ing time alignment, outlier handling, and unit standardization.

245 **Data Preprocessing** Raw datasets required minimal yet essential processing to form a consistent, easy-to-use resource. In par-  
ticular, PWS are user-maintained and may not be calibrated to standardized protocols, and each sensor logs data on different  
schedules: NYC Mesh devices record at 56 s or 64 s intervals (with occasional missing samples or errors), while WUnder-  
ground PWS provide readings every 5–15 min. Because these measurements were not inherently synchronized, we applied the  
following steps to ensure alignment and standardization for analysis:

- 250
- **Time Alignment:** Each source was resampled to a fixed interval—1 min for Mesh sublinks, 5 min for WUnderground  
PWS, and 30 min for airport data—to provide a consistent temporal resolution across all measurements.
  - **Outliers and NaN Handling:** Physically implausible outliers and missing measurements were replaced with NaN. Minor  
gaps (up to two consecutive samples) were interpolated to maintain continuity, while longer gaps remained as missing  
data.

## 255 3 Data Analysis

This section examines how different weather conditions in NYC affect OpenMesh sublinks with varying carrier frequencies and  
path lengths, thereby demonstrating the network’s potential for urban environmental monitoring. Fig. 4 shows five months of  
data (10 Nov 2023–10 Apr 2024): RSL measurements (dBm) from a 69 GHz, 1.8 km sublink plotted against mean precipitation  
recorded by a nearby PWS. Peaks in precipitation rate ( $\text{mm h}^{-1}$ ) coincide with sharp RSL drops, confirming a strong inverse  
260 relationship between precipitation intensity and signal strength. The shaded interval marks an NYC Mesh outage that produced  
a data gap (see Sect. 2.1.3).

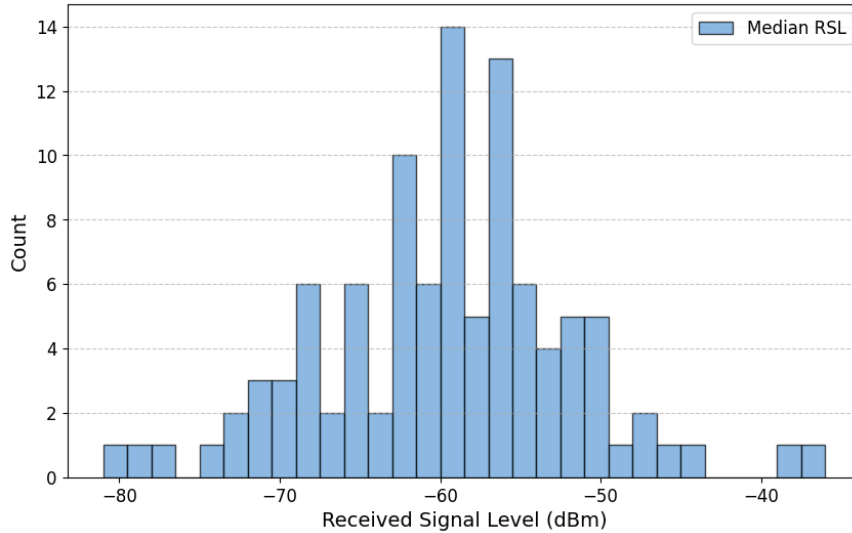


**Figure 5.** RSL distribution (dBm) across sublinks

### 3.1 Rain-Induced Attenuation

The  $k$ - $R$  relationship describes rain-induced attenuation  $\gamma$  as a function of the rainfall rate  $R$ , typically expressed as (ITU-R P.838, 2005; Olsen et al., 1978):

$$265 \quad \gamma_r(R) = k R^\alpha, \quad (2)$$

where  $k$  is an attenuation coefficient and  $\alpha$  is an exponent that depend on factors such as signal frequency, polarization and the drop-size distribution. The total rain-induced attenuation  $A_r(t)$  along the link's propagation path can then be written as:

$$A_r(t) = \int_{\text{path}} \gamma_r(R(\ell, t)) d\ell \approx k \bar{R}(t)^\alpha L_e, \quad (3)$$

270 Here,  $\gamma_r(R(\ell, t))$  is the local specific attenuation ( $\text{dB km}^{-1}$ ) at rain rate  $R(\ell, t)$ , and the integral sums the total attenuation along the path. Assuming uniform rainfall along the path, the integral simplifies to a power-law relation in which the path-averaged rainfall rate  $\bar{R}(t)$  and effective link length  $L_e$  govern attenuation—an approximation widely used in radio communications and meteorological estimation. Extended versions of the ITU-R model add location-tuning parameters and refined path-correction factors, improving accuracy across varied climates and better capturing the specific meteorological nuances of diverse regions (Alozie et al., 2022; Samad et al., 2021). While several environmental factors—rain, fog, oxygen absorption  
 275 in dry air, and solid precipitation such as snow—can attenuate mmWave signals across most frequencies (Fig.1b), the raw RSL trace with PWS records in Fig.4 shows that liquid precipitation, often associated with heavy rainfall and causing losses exceeding 30 dB at peak, is the dominant source of attenuation whenever it occurs.



**Table 2.** 15-min window statistics (in dB km<sup>-1</sup>) under Dry vs. Wet intervals.

Freq Band	Window Mean $\Delta\bar{A}_{15}$				Window Std $\bar{\sigma}_{15}$			
	Dry mean	Dry med.	Wet mean	Wet med.	Dry mean	Dry med.	Wet mean	Wet med.
5 GHz	0.07	0.00	0.78	0.31	0.61	0.56	0.64	0.59
23 GHz	0.02	0.00	0.58	0.38	0.27	0.35	0.38	0.46
60 GHz	<b>0.14</b>	0.00	1.26	0.69	<b>1.00</b>	<b>0.92</b>	<b>1.05</b>	<b>0.98</b>
70 GHz	0.06	0.00	<b>2.28</b>	<b>0.91</b>	0.34	0.38	0.90	0.64

### 3.2 Processing Steps and Metrics

**Baseline Reduction.** Wireless links typically experience stable, slow changing path loss under dry conditions. However, transient weather phenomena (e.g., precipitation) introduce additional attenuation. Our dataset comprises RSL measurements, from which we derive attenuation metrics. To quantify the added attenuation beyond baseline conditions, we define:

$$\Delta A(t) = RSL_{\text{baseline}}(t) - RSL(t), \quad (4)$$

Where  $RSL(t)$  is the measured power at time  $t$  and  $RSL_{\text{baseline}}(t)$  denotes the nominal dry-weather signal level. Fig. 5 shows the histogram of median RSL across sublinks, ranging from about  $-80$  dBm to  $-40$  dBm. These variations stem from differences in transmit power, link distance, antenna gains, and operating frequencies. The median value can serve as a simple, constant baseline reflecting typical non-rain levels. However, to account for temporal changes in these factors, we adopt a dynamic, two-step approach: (1) identify consecutive dry intervals using the nearest PWS, and (2) within those intervals, compute the baseline as the three-hour median RSL, ensuring a robust, recent dry-weather reference.

**Path-Averaged Attenuation.** Let  $L$  (km) denote the link length, i.e., the distance between the transmitter and receiver. The path-averaged attenuation  $\Delta\bar{A}(t)$  is defined by normalizing the total measured attenuation above the baseline by  $L$ :

$$\Delta\bar{A}(t) = \frac{\Delta A(t)}{L}, \quad (5)$$

where  $\Delta A(t)$  is the total measured attenuation at time  $t$ . Specifically, the total attenuation  $A(t)$  along the path represents the cumulative effects experienced by the signal along its entire electromagnetic propagation path. Here, we simplify these accumulated effects by letting the effective link length  $L_{\text{eff}}$  approximate the direct distance  $L$ , thereby facilitating statistical comparisons among links of different lengths by minimizing distance-dependent biases.

**Pairing Link-PWS Data.** In our analysis, we correlate signal measurements from sublinks with precipitation collected by nearby PWS. Each sublink is paired with spatially averaged PWS rainfall measurements from stations located within 3 km distance. This method gathers a wide range of nearby measurements, reducing possible errors from individual PWS, and still reflect the local patterns by considering data only from nearby stations (Overeem et al., 2011).

**Aggregated Statistics.** To capture both short-term fluctuations and longer-term rainfall trends, we aggregate meteorological and attenuation data over different time intervals. Instantaneous measurements at time  $t$  refer to the native sensor temporal scales (e.g., 1-min for signal measurements and 5-min for meteorological data). We define  $\Delta A_m(t)$  as the attenuation averaged over an  $m$ -minute interval ending at  $t$ . For example, 15-minute  $\Delta A_{15}(t)$  and 60-minute  $\Delta A_{60}(t)$  aggregations reflect

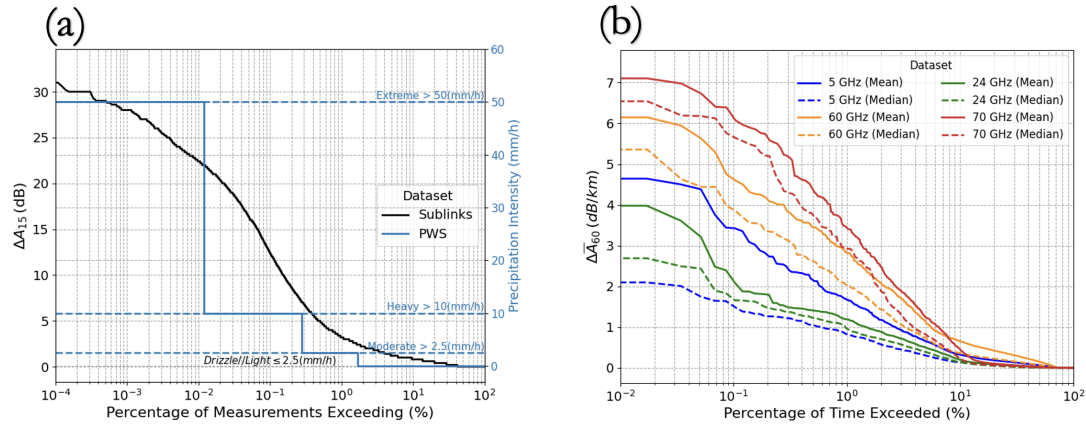


**Figure 6.** Exceedance probability plots. The x-axis shows the fraction of samples that exceed the y-axis value. (a) Portion of NYC Mesh and WUnderground measurements surpassing each intensity with precipitation binned into intensity categories. (b) Hourly aggregated mean and median attenuation across all sublinks, grouped by carrier frequency, illustrating overall trends over the study period.

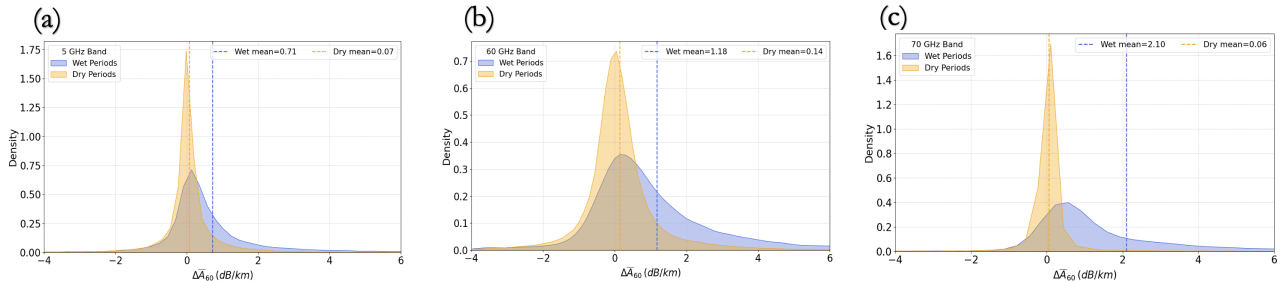


**Figure 7.** Path-averaged attenuation distributions for wet (blue) and dry (orange) periods across frequency bands. Each plot shows the density of hourly path-averaged attenuation ( $\text{dB km}^{-1}$ ).

different insights into rainfall patterns. Different temporal aggregation scales provide varied insights: shorter intervals, such as minutes-scale data, effectively capture rapid changes and rapid hydrological responses typical in urban environments but are influenced by the aggregation time itself (Berne et al., 2004; Lompi et al., 2022), whereas hourly aggregations provide broader precipitation and attenuation trends.

### 3.3 Precipitation and Link Attenuation

#### 3.3.1 Sample Exceedance Distributions

The OpenMesh dataset spans eight months, covering both winter and spring, and captures a broad spectrum of precipitation—from light drizzles to heavy intensities, including occasional ice and snowstorms. This variety provides a rich foundation for examining how diverse weather events are recorded in the OS dataset and how they influence link attenuation patterns. This

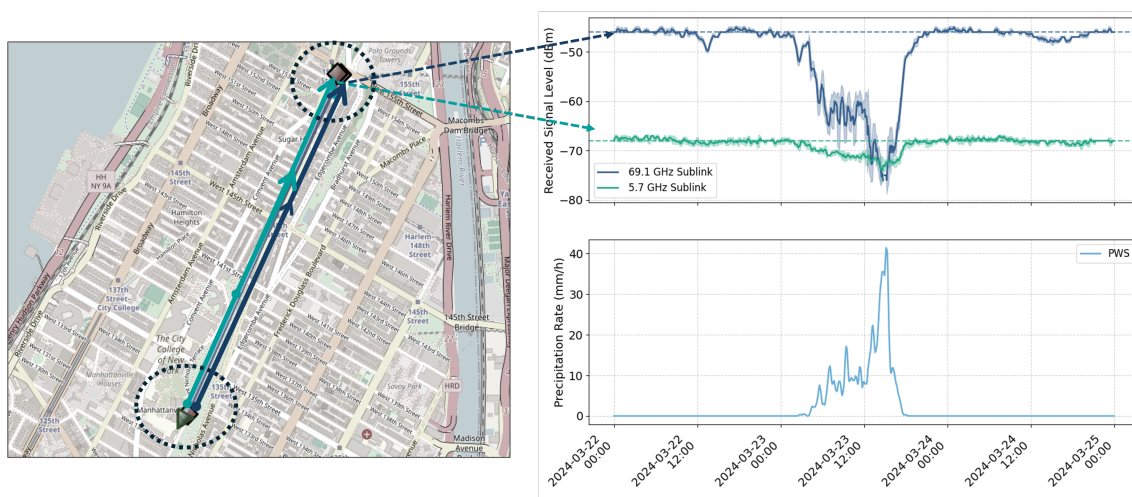


**Figure 8.** Multi-Band Link Demonstration: The sublink at 69 GHz (blue) experiences larger attenuation than the 5.7 GHz (green) channel, as shown by the upper-right RSL plot. The lower-right plot displays average precipitation rates recorded by nearby PWS. © OpenStreetMap contributors 2025. Distributed under the Open Data Commons Open Database License (ODbL) v1.0.

diversity is illustrated in Fig. 6, which shows exceedance probability curves for precipitation (from WUnderground) and sub-link attenuation (from NYC Mesh), based on the observed values. These plots depict the fraction of measurements exceeding various thresholds for 15-minute aggregation, highlighting the proportion of low to extreme conditions in each dataset, and thereby presenting the sample complementary cumulative distribution function (CCDF) of the dataset. Fig. 6a represents the sample CCDF for both raw datasets presenting the actual recorded values, with no additional processing or adjustments, thus reflecting the full range of measured values yet not accounting for missing data gaps. Precipitation intensities are categorized into discrete ranges following (WMO, 2018).

The plotted attenuation values represent increments above a baseline, and most samples (99%) remain below 3 dB, indicating stable link performance under predominantly dry conditions. These dry conditions are evident in over 90% of the measurements—about 90% register zero precipitation, and approximately 98% fall under drizzle or light intensities ( $< 2.5$  dB km<sup>-1</sup>).

Around 0.5% of attenuation values exceed 5 dB, typically driven by weather-related events. Moderate precipitation intensities (2.5–10 dB km<sup>-1</sup>) comprise roughly 0.5–2% of PWS measurements, while higher intensities (10–50 dB km<sup>-1</sup>) occur in only about 0.01–0.1%. The more extreme values ( $> 50$  dB km<sup>-1</sup>), often associated violent, localized showers that PWS capture thanks to their dense coverage, may also arise from measurement inaccuracies (e.g., sensor overestimation). Observed attenuation occasionally reaches about 30 dB in rare cases. However, extreme rainfall often leads to link collapses, resulting in missing or NaN measurements rather than high recorded values. These collapses depend on various factors—such as device hardware, link frequency, and link length—and typically occurs at higher attenuation values associated with extreme or heavy rainfall.

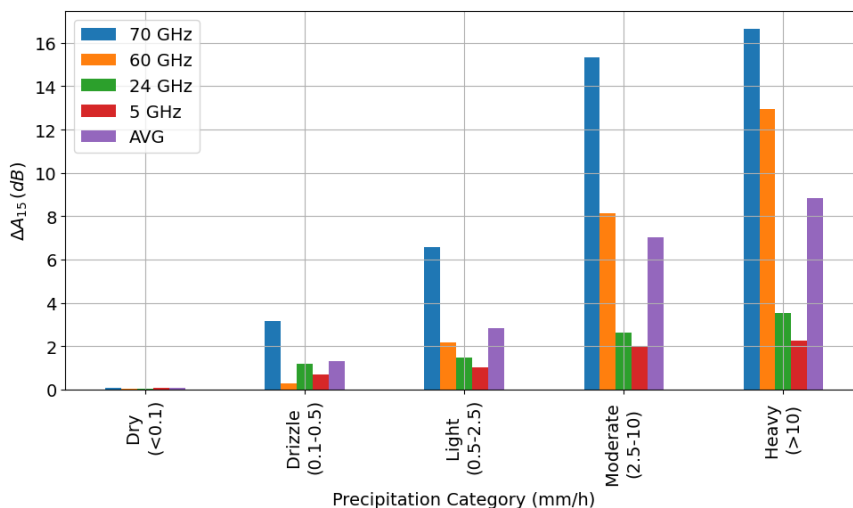


**Figure 9.** Attenuation for  $\sim 1.5$  km sublinks for various frequency band, grouped by precipitation intensity.

### 3.3.2 Attenuation Across Frequency Bands

Different frequency bands inherently experience varying attenuation characteristics, so we analyze multiple bands in the NYC Mesh sublinks to capture these differences. To mitigate the influence of link length, we present normalized attenuation values in the sample CCDF for each band.

335 Fig. 6b shows hourly aggregated statistics (mean and median) of path-averaged attenuation  $\Delta\bar{A}_{60}(t)$ , highlighting the frac-  
 tion of time each attenuation threshold is surpassed. These mean and median values are calculated from the available mea-  
 surements of all sublinks within each hour, reducing the impact of localized extreme attenuation that may appear in individual  
 sublink measurements to show overall attenuation patterns. Higher frequency bands (60 and 70 GHz) exhibit higher exceedance  
 probabilities at larger attenuation values compared to lower frequency bands (5 and 24 GHz), reflecting their increased sensi-  
 340 tivity to precipitation. Notably, the mean path-averaged attenuation for the 5 GHz band appears higher than that for the 24 GHz  
 band—an artifact resulting from the inclusion of shorter sublinks and normalization effects at 5 GHz, which bias the normal-  
 ized values upward. Moreover, the 5 GHz band comprises the largest number of sublinks in the dataset (55 sublinks), capturing  
 broader spatial coverage and a richer temporal context that encompasses most weather events. **Wet vs. Dry Periods.** Fig. 7  
 displays histograms of the path-averaged attenuation,  $\Delta\bar{A}_{15}$ , computed from all 15-minute measurement windows across NYC  
 345 Mesh sublinks. These histograms highlight differences between dry and wet periods for the 5, 60, and 70 GHz bands. Table 2  
 summarizes the mean and median  $\Delta\bar{A}_{15}$  values and the path-averaged standard deviation (std),  $\bar{\sigma}_{15}$ , which quantifies the 15-  
 minute window variability across all frequency bands in wet versus dry intervals (with wet periods determined from local PWS  
 data). The derived path-averaged standard deviation,  $\bar{\sigma}_W$ , quantifies the signal’s variability within each time window  $W$ , with  
 low variability in dry periods and higher fluctuations during rainy periods that enable rain detection Schleiss and Berne (2010).

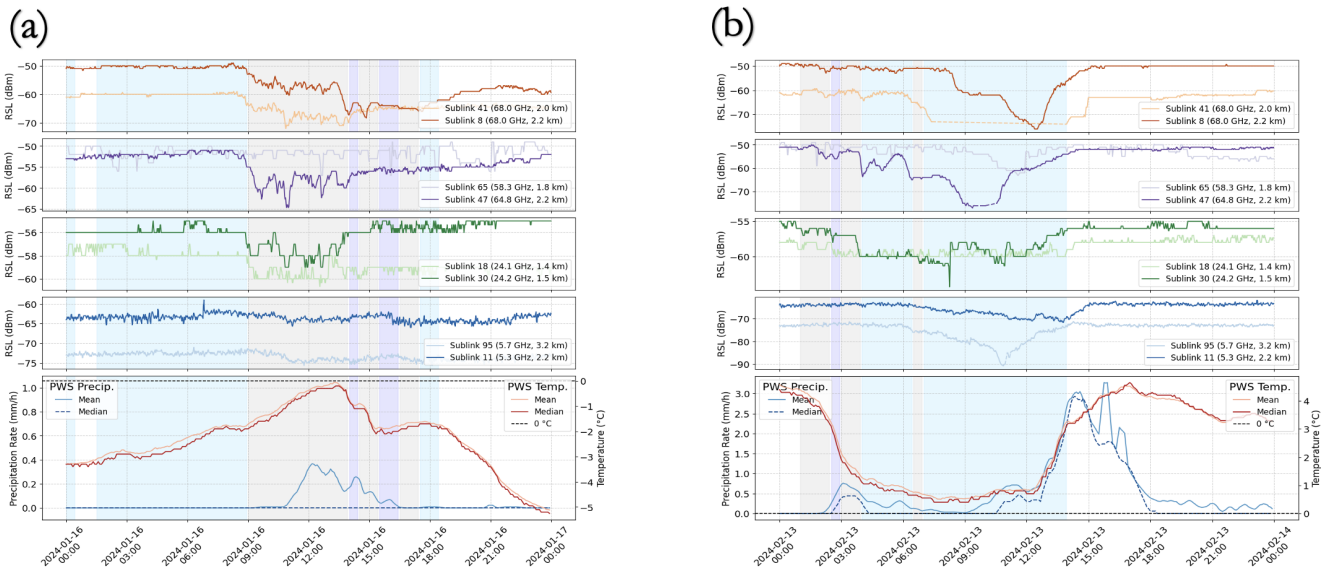


**Figure 10.** On two illustrative snowfall days (15 Jan and 10 Feb 2024), this figure shows RSL traces from two OpenMesh sublinks per frequency band alongside PWS precipitation rate ( $\text{mm h}^{-1}$ ) and temperature ( $^{\circ}\text{C}$ ). Colored shading indicates precipitation type reported by the airport WS: snowfall (cyan), mixed rain/snow (gray), rainfall (blue), and dry (white).

350 Under dry conditions, all frequency bands exhibit symmetrical distributions centered around zero, indicating that the measured values cluster around the corresponding sublink baseline level (Equation 4). In contrast, wet-period distributions are right-skewed with positive attenuation values, highlighting an additional attenuation component due to rainfall. Specifically, the 70 GHz band shows the clearest separation between wet and dry periods, with noticeably higher attenuation in wet conditions. The 5 GHz band, however, demonstrates overlap between wet and dry distributions, making it more difficult to differentiate  
 355 solely by attenuation. Meanwhile, the 60 GHz band not only exhibits high attenuation during wet periods but also relatively high values in dry periods, underscoring its susceptibility to non-rain influences (see Fig. 1b). It also experiences the highest std values, showing notably high fluctuations in dry conditions, indicative of inherently noisier signal behavior.

For a more direct comparison of frequency bands and to reduce the effect of normalization, we show the total attenuation statistics for links of the same length. In Fig. 9, we present mean attenuation across all frequency bands using one representative  
 360 sublink per band ( $\sim 1.5$  km). The results indicate that higher-frequency bands exhibit greater attenuation across all rainfall categories, reflecting (i) elevated attenuation patterns under higher intensities for every band and (ii) stronger rain-induced attenuation at higher frequencies. Rainfall categories for each sublink are determined by averaging the nearest PWS data at 15-minute intervals to ensure consistent time windows.

While Fig. 6c suggests that the 60 GHz band can experiences less weather-induced attenuation than the 5 GHz and 24 GHz  
 365 bands, path attenuation is heavily influenced by link length: most 24 GHz sublinks exceed 1 km (up to 4 km), whereas most 60 GHz sublinks are shorter in our dataset.



To compare different frequency bands under identical rain conditions, Fig. 8 shows a three-day interval (03/23–03/24) with a rain event measured by a local PWS and a multi-band link running from the City College of New York to a northern endpoint in Harlem. This channel consists of two sublinks operating at a high frequency (69 GHz) and a low frequency (5.7 GHz), respectively, which follow similar paths and experience the same weather conditions yet display markedly different attenuation levels. During this period, heavy rainfall was recorded on March 23, corresponding to substantial attenuation in both sublinks. At the peak of the rain event, the 69 GHz sublink undergoes nearly 30 dB of additional path loss—enough to cause sublink collapse—while the 5.7 GHz sublink incurs only around 5 dB of loss. These observations motivate the use of multi-band links in certain scenarios: the 5 GHz band can serve as a backup during high-attenuation events, while the increased sensitivity of higher-frequency links can be leveraged to more precisely detect weather phenomena such as precipitation.

### 3.4 Beyond Rain: Snowfall Sensing

Sensing non-liquid precipitation (e.g., snow, ice, or sleet) remains challenging for conventional gauges and for PWS lacking dedicated snow sensors. Many standard WS—while they do register precipitation—often rely on unheated rain gauges that under-measure freezing or frozen precipitation, potentially leading to inaccuracies or lagged readings. Therefore, additional datasets and sensors—such as wireless communication links—can help fill observational gaps by detecting snowfall events more directly, thus providing valuable insights into these phenomena.

Table 3.4 summarizes daily snowfall records for Winter 2024 at KJFK, KLGa, and Central Park (KNYCCP). Initial accumulations stayed under 1cm in early January and up to 5cm in subsequent events, while mid-February saw heavier snowfall reaching 15.75cm at KJFK. Note that Manhattan’s only snowfall measurements come from a single site in Central Park, reporting only daily totals—further underscoring the need for more real-time sensing solutions.

**Table 3.** NOAA Daily Snowfall Depth Measures.

Date	KJFK (cm)	KLGA (cm)	KNYCCP (cm)
2024-01-06	0.25	0.76	0.51
2024-01-15	1.78	0.76	1.02
2024-01-16	3.30	5.08	3.30
2024-01-19	0.76	3.30	1.02
2024-02-13	10.67	8.38	8.13
2024-02-17	15.75	8.38	5.08

Fig. 10 shows two snowfall events in NYC during Winter 2024: one on 16 January with moderate daily accumulations of about 39 mm, and another on 13 February with heavier accumulations near 90.6 mm. The bottom panel plots mean and median precipitation and temperature from local PWS, indicating overall weather conditions in the region. Above it, four panels present RSL measurements for sublinks grouped by frequency band, with two sublinks per band.

The first row (orange) includes 68 GHz mmWave sublinks (~ 2 km), the second row (purple) shows other ~ 60 GHz band links (~ 2 km), the third row (green) highlights ~ 1.5 km, 24 GHz links, and the fourth row (blue) covers lower frequencies



(5–6 GHz). All plots are color-shaded based on airport station categories to reflect the recorded 'condition' at each interval: dry (no precipitation), wet (rain reported by both stations), wintry mix (partially frozen, sleet, or mixed precipitation), and snow. Few observations are evident from the snowy days examples.

395 **Attenuation Across Frequency Bands** As expected, higher frequencies suffer greater weather-induced attenuation under freezing conditions. During the lighter 16 January snowfall, the 5 GHz and 24 GHz links dropped only 3–4 dB, while the 60 GHz and 70 GHz links lost up to 15 dB. In the heavier 13 February event, even lower-frequency sublinks (e.g., 11 and 30) dipped by about 10 dB, whereas the highest-frequency sublinks (e.g., 8 and 47) collapsed entirely, underscoring the extreme vulnerability of mmWave bands.

400 **Freezing Conditions Misalignments.** During the 16 January event, local PWS did not register precipitation until after 11:00, even though airport stations indicated snow earlier and NOAA data reported a total of 39 mm. This discrepancy suggests that WUnderground PWS—primarily geared toward liquid precipitation—either failed to record or significantly under-measured the snow event. For instance, while WUnderground stations collectively reported under 1 mm of total precipitation, NOAA recorded 38.9 mm of snowfall depth and 9 mm of precipitation. In contrast, high-frequency sublinks registered pronounced  
405 attenuation by 9:00, despite negligible PWS readings, underscoring the links' heightened sensitivity to non-rain conditions. A similar delay occurred in the February snowfall event: the strongest sublink attenuations aligned with reported snowy intervals, whereas PWS measurements remained low or indicated “dry” until after 13:00, even as airport stations and stable link-attenuation levels indicated ongoing snow. This misalignment likely stems from rising temperatures melting snowfall or ice on the gauges, leading to underestimation during snow and overestimation during the melting phase. Meanwhile, sublinks  
410 stayed consistent with airport snow indicators, further revealing the limitations of PWS in freezing conditions.

**Snow-Types Impact.** Near-surface precipitation classification from the WMO codes (WMO, 2018; Fierz et al., 2009) ranges from damp or rime-covered surfaces to slush, dry snow, or compacted ice, each with distinct liquid-water content. Among these, “dry” vs. “wet” snow can dramatically alter microwave attenuation due to partial melting (Mätzler, 1987). Because meteorological factors such as temperature, humidity, and air pressure strongly shape snow microstructure, a more detailed  
415 analysis is needed to interpret link attenuation under these varying conditions.

In our observations, subfreezing temperatures (below  $-2^{\circ}\text{C}$ ) during the January event yielded minimal sublink attenuation during snowfall, suggesting that dry snow is effectively transparent to microwave signals. In contrast, the warmer ( $0\text{--}2^{\circ}\text{C}$ ) February storm produced significantly higher signal losses—sometimes causing full link collapses—implying “wet” snow, where partial melting leads to greater attenuation.

420 **Wet/Frozen Antenna Effects.** Wet and frozen antenna surfaces can introduce additional attenuation in microwave link signals, sometimes dominating overall measurement errors (Schleiss et al., 2013; Ostrometzky et al., 2017; Kozak et al., 2021). This effect often manifests as prolonged signal reductions even after precipitation stops, especially under freezing conditions where moisture or ice remains on antenna surfaces. For instance, sublinks 41, 8, 47, and 18 in our January event did not promptly return to baseline RSL levels despite colder, drier weather—indicating that residual moisture or ice on antennas delayed full  
425 signal recovery.

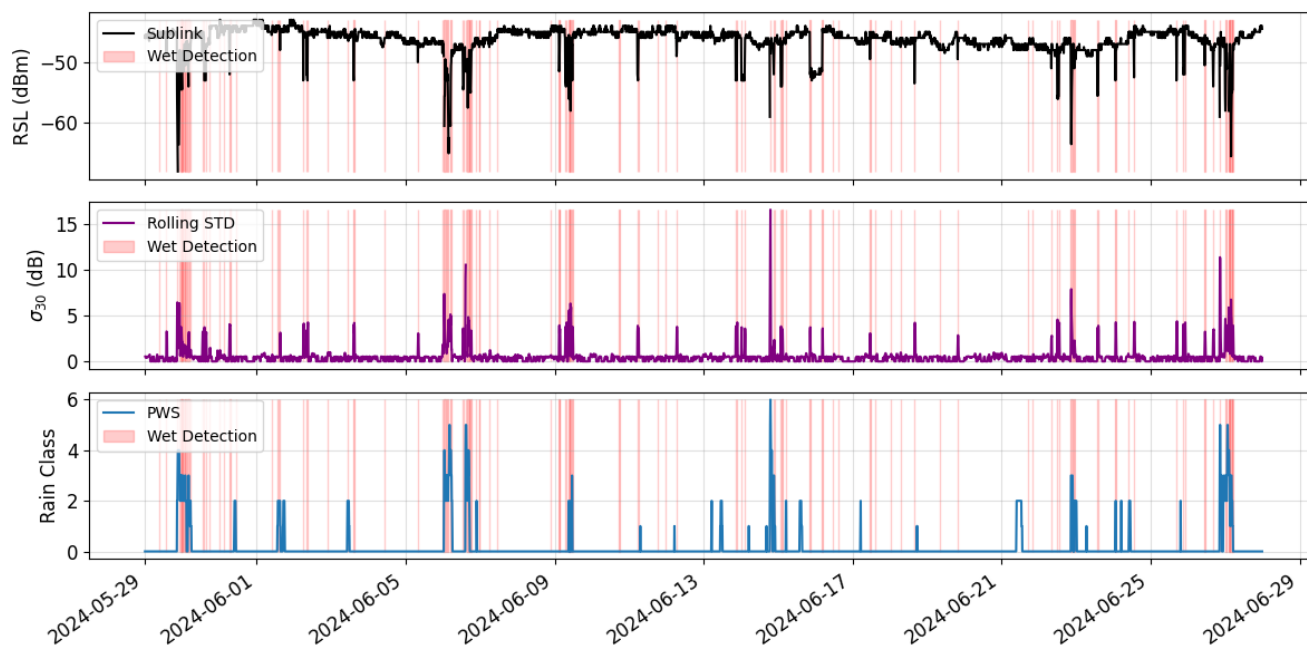


**Figure 11. Rain Detection Example:** One-month sublink sample illustrating RSL (top), the corresponding rolling STD (middle), and PWS-based rain intensity (bottom). Red-highlighted intervals indicate wet detections triggered by elevated STD values.

These examples demonstrate that wireless links detect both liquid and frozen precipitation effectively, particularly under snowy or mixed conditions—though certain low-temperature snow types appear relatively transparent. Meanwhile, wet or freezing antennas can distort signal levels and require further analysis to distinguish ice buildup from actual precipitation. Despite these challenges, wireless links remain a promising solution for bridging measurement gaps and enhancing real-time snow detection.

## 4 Applications

In this section, we demonstrate the applicability OS of rainfall using a sublink from 70 GHz band, which has been shown to be highly sensitive to weather events. We focus on two main tasks: (i) rain detection (wet-dry classification) and (ii) rain intensity estimation. We present results from a 69 GHz sublink spanning 6.9 km, illustrating the ability to classify and detect precipitation solely from signal strength measurements.

### 4.1 Rain Detection

The task of detecting rainfall can be framed as a binary decision—distinguishing rain from dry periods—using only wireless signal measurements. Here, we employ the RSL of a 69 GHz sublink as a case study over a one-month interval. Traditional

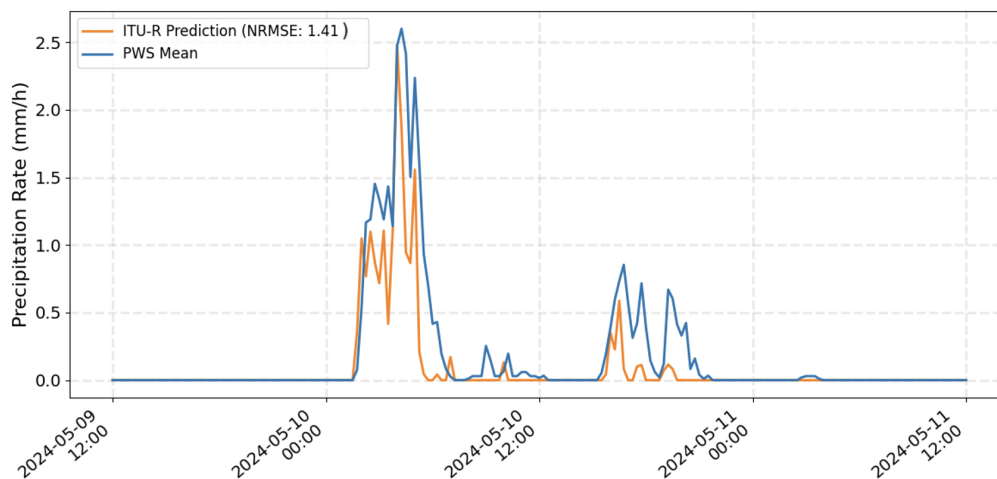


**Figure 12.** Comparison of ITU-R–based rainfall estimates from a 69 GHz microwave sublink with PWS measurements over a two-day precipitation event, highlighting their close agreement and demonstrating the feasibility of using sublinks for rainfall sensing.

detection methods often rely on thresholding-based algorithms, whereas more recent machine-learning approaches (e.g., (Habi  
440 and Messer, 2018)) aim to learn signal patterns directly. In our analysis, we adopt the rolling standard deviation (STD) method  
from Schleiss and Berne (2010), applying a 30-minute window to flag significant RSL fluctuations indicative of rain-induced  
attenuation.

Fig 11 depicts a continuous record for June 2024, comparing the sublink measurements to data from a nearby PWS. The top  
plot shows the RSL (black line); the middle plot displays its 30-minute rolling STD (purple line); and the bottom plot indicates  
445 PWS-derived rain intensity classes. Red bars mark “wet” intervals as determined by the rolling-STD threshold. Overall, these  
wet flags align well with periods of higher PWS intensities, especially during intense rainfall events. Still, some inconsistencies  
arise, including false alarms (wet detections absent in the PWS) and missed detections (precipitation in the PWS not reflected  
in the RSL). These discrepancies could stem from sensor calibration issues, localized precipitation effects not captured by the  
PWS, or inherent limitations of simple threshold-based algorithms. Nevertheless, the strong agreement during major events  
450 underscores the viability of sublink-based rainfall detection in opportunistic sensing scenarios.

## 4.2 Rain Estimation

We employ the ITU-R model to relate specific attenuation to rainfall rate via a power-law relationship (Eq. (3)), where wireless  
links capture signal attenuation caused by rain and convert it into rainfall intensity estimates using predetermined parameters  
(ITU-R P.838, 2005). Concretely, the model maps the observed sublink attenuation,  $\Delta A(t)$  (in dB), to the mean precipitation  
455 ( $\text{mm h}^{-1}$ ) measured by nearby PWS. Fig. 12 shows a two-day precipitation event, comparing the sublink-derived rainfall  
intensity (orange) to the mean PWS measurements (blue). ITU-R parameters translate rain-induced path attenuation (with wet-



antenna correction following (Schleiss et al., 2013)) into rainfall estimates. To avoid false positives during dry periods, we apply a rolling standard-deviation threshold for rain detection and assign zero rainfall whenever no wet flag is raised.

Overall, the sublink closely tracks the timing and magnitude of the PWS measurements, with minor underestimation at lower intensities. We quantify accuracy via the normalized RMSE (NRMSE)—the ratio of the RMSE between estimated and observed rainfall to the total observed rainfall over the interval—which confirms strong agreement. These results demonstrate the feasibility of using 69 GHz sublinks for reliable rainfall sensing under warm, liquid-precipitation conditions. Extension to snow or hail would require additional model adaptations and encourages further research.

## 5 Discussion

We introduced the OpenMesh dataset to demonstrate the feasibility of opportunistic sensing for high-resolution, urban-scale weather monitoring using NYC Mesh’s multi-band links. The observed attenuation patterns across frequencies generally align with established theoretical models, showing pronounced rainfall sensitivity over various bands and even detecting frozen precipitation that can be missed by unheated PWS. Our snow-event analyses further highlight how “wet” versus “dry” snow can drastically alter signal attenuation, while frozen antenna surfaces emphasize the importance of non-rain processes on link performance.

**5 GHz Sublinks.** Lower-frequency, 5 GHz links in NYC Mesh are widely used for everyday internet backhaul. Most are relatively short, but those spanning greater distances still exhibit noticeable attenuation during moderate-to-heavy rainfall. Owing to their extensive deployment in NYC, these links can complement higher-frequency sublinks, for instance in establishing baseline calibrations or detecting broader weather patterns.

**60 GHz Sublinks.** The 60 GHz band is largely unlicensed—which simplifies deployment and enables high-throughput, mainly with short-range links thanks to the wide bandwidth available at these frequencies. However, strong oxygen absorption (see Fig. 1b) severely limits communication range and introduces additional attenuation factors, a critical consideration for hydrological sensing. Our analysis (Figs. 6b, 7; Table 2) shows that—even in dry conditions—60 GHz links exhibit baseline noise likely tied to atmospheric effects, complicating precise estimation of rain-induced attenuation. Therefore, Additional filtering and more advanced analysis are required to assess the 60GHz band’s usability for urban sensing.

**70 GHz Sublinks.** Among the NYC Mesh links, the 70 GHz band exhibits particularly strong weather sensitivity but less baseline variability than 60 GHz, enabling clearer distinctions between wet and dry periods. This heightened responsiveness aids in detecting both mild and intense rainfall (including wet snow), but also risks link collapses during severe downpours, resulting in missing data. NYC Mesh often pairs these high-capacity mmWave links with lower-frequency backups (e.g., 5 GHz) at critical connection points—an operational redundancy that enhances communication reliability and opens opportunities for multi-band meteorological sensing (Fig. 8). We demonstrated rain-detection and rainfall-intensity algorithms using 70 GHz links, illustrating how they can effectively sense precipitation, although localized rainfall or underreporting of frozen conditions may lead to discrepancies with PWS data.



**PWS Dataset.** Our study also incorporates extensive WUnderground PWS coverage, offering near-real-time data across dense  
490 urban neighborhoods. Though these unheated tipping-bucket gauges may under-report or lag in detecting freezing precipitation,  
they remain a cost-effective baseline for rainfall studies and a valuable cross-check for opportunistic sensors. Further research  
on quality control and filtering (de Vos et al., 2019) could strengthen the reliability of PWS in weather sensing facilitate  
integration of OS observations.

Altogether, these findings underscore the importance of merging OS datasets (e.g., NYC Mesh) with official sources (e.g.,  
495 airport stations, NOAA) for improved calibration and robust, high-resolution precipitation monitoring. Looking ahead, the  
growing deployment of 5G/6G networks and principles will likely increase the spatial density and spectral diversity of wireless  
infrastructure, promising richer, real-time urban weather sensing and broader applications.

## 6 Data availability

The OpenMesh dataset—comprising NYC Mesh wireless link measurements—is publicly available under the Creative Com-  
500 mons Attribution 4.0 License (CC BY 4.0) on Zenodo, DOI: <https://doi.org/10.5281/zenodo.15268340> (Jacoby et al., 2025).  
The measurements are provided in NetCDF format compliant with the OpenSense CML specifications v1.1 (standardized  
naming, units, and metadata conventions) and accompany a white paper on standards and conventions for opportunistic  
rainfall-sensor data (Fencl et al., 2023). Supplementary meteorological observations used in the paper— from WUnderground  
and NOAA—are freely accessible through their respective online platforms and together present the full database used in this  
505 paper. Subsequent revisions will be updated as new Zenodo versions with separate DOIs; the Concept DOI always resolves to  
the latest.

## 7 Code availability

Core scripts and notebooks are available at <https://github.com/drorjac/OpenMesh>. The repository currently contains exam-  
ples of data reading and analysis and is actively being expanded with additional modules and results. The NetCDF dataset  
510 aligns with the OpenSense specification and interoperates with the opportunistic-hydrology codebase at [https://github.com/  
OpenSenseAction](https://github.com/OpenSenseAction). Community contributions are welcome.

## 8 Concluding Remarks

Recent open-data initiatives for meteorological monitoring increasingly leverage opportunistic sensors from diverse communi-  
cation platforms. As next-generation wireless networks adopt higher-frequency bands, community-driven infrastructures—like  
515 NYC Mesh—present a promising avenue for capturing high-resolution precipitation data at minimal additional cost. Through-  
out this study, we have highlighted both the potential and the challenges in repurposing such link measurements for weather  
sensing; while further refinement is needed, the widespread deployment of short, high-frequency links already underway sug-  
gests that a move from demonstration to operational implementation is achievable.



We also cross-referenced these community-collected signals with PWS data, primarily sourced from WUunderground, demon-  
520 strating both close alignment in certain precipitation events and notable misalignments (e.g., during snowfall), underscoring the  
importance of careful calibration and open-data collaboration. These highlight the value of innovative, in-city wireless datasets  
and underscore the need for stronger partnerships among mesh operators, municipal agencies, and hydrometeorological insti-  
tutions, ensuring that such data can be seamlessly incorporated into existing monitoring systems

Once these practical hurdles are addressed in future research and operational plans, near-real-time, hyper-local precipita-  
525 tion measurements could significantly enhance climate resilience efforts. We anticipate that volunteer-driven mesh networks  
will become a reliable asset in urban meteorological sensing, complementing conventional instruments and fostering stronger  
community engagement in environmental observation.

*Author contributions.* DJ conceived the overall dataset framework, led software development, performed data preprocessing, conducted  
formal analysis and visualization, and wrote the original manuscript draft. SY contributed to software development, data curation, and  
530 reviewed and edited the manuscript. QH contributed to data collection, analysis, and implementation. ZH contributed to software development  
and data collection. RJ provided access to network resources, contributed to data validation, and reviewed the manuscript. JO, IK, GZ, and  
HM supervised the research, contributed to methodology, and critically reviewed and edited the manuscript.

*Competing interests.* The authors declare that they have no conflict of interest.

*Acknowledgements.* We thank the NYC Mesh community for sharing their network data and offering great support. Their volunteer-run  
535 network is key to this project and helps open the door to future work that improves connectivity, research, and our society. Special thanks to  
Rob Johnson for his constant support and collaboration, and to Olivier Morf for his technical help. We also thank the Columbia University  
undergraduates who helped build the data pipeline, especially Muchen Sui and Weijie Wang for managing the database. This research was  
supported in part by NSF-BSF grant CNS-1910757 and NSF grant EEC-2133516; by the Next Generation Internet (NGI) initiative, which  
envisions an open, interoperable, and ethically driven Internet of the future; and by NGI Enrichers under EU-funded project No. 101070125.



## 540 References

- Action, O.: New Open CML Dataset from Italy: OpenRainER, <https://opensenseaction.eu/news/new-open-cml-dataset-from-italy-openrainer/>, [Online; accessed 2023-09-09], 2023.
- Alozie, E., Abdulkarim, A., Abdullahi, I., Usman, A. D., Faruk, N., Olayinka, I.-F. Y., Adewole, K. S., Oloyede, A. A., Chiroma, H., Sowande, O. A., et al.: A review on rain signal attenuation modeling, analysis and validation techniques: Advances, challenges and future direction, *Sustainability*, 14, 11 744, 2022.
- 545 Andersson, J., Olsson, J., van de Beek, R. C., and Hansryd, J.: OpenMRG: Open data from Microwave links, Radar, and Gauges for rainfall quantification in Gothenburg, Sweden, *Earth System Science Data*, 14, 5411–5426, 2022.
- Arvas, M. and Alsunaidi, M.: Analysis of oxygen absorption at 60 GHz frequency band, in: 2019 IEEE International Symposium on Antennas and Propagation and USNC-URSI Radio Science Meeting, pp. 2127–2128, IEEE, 2019.
- 550 Berne, A., Delrieu, G., Creutin, J.-D., and Obléd, C.: Temporal and spatial resolution of rainfall measurements required for urban hydrology, *Journal of Hydrology*, 299, 166–179, 2004.
- Bi, K., Xie, L., Zhang, H., Chen, X., Gu, X., and Tian, Q.: Accurate medium-range global weather forecasting with 3D neural networks, *Nature*, 619, 533–538, 2023.
- Bojinski, S., Blaauboer, D., Calbet, X., De Coning, E., Debie, F., Montmerle, T., Nietosvaara, V., Norman, K., Bañón Peregrín, L., Schmid, F., et al.: Towards nowcasting in Europe in 2030, *Meteorological applications*, 30, e2124, 2023.
- 555 Castello, P., Muscas, C., Pegoraro, P. A., and Sulis, S.: Improved Fine Particles Monitoring in Smart Cities by Means of Advanced Data Concentrator, *IEEE Transactions on Instrumentation and Measurement*, 70, 1–9, <https://doi.org/10.1109/TIM.2020.3031987>, 2021.
- Chwala, C. and Kunstmann, H.: Commercial microwave link networks for rainfall observation: Assessment of the current status and future challenges, *Wiley Interdisciplinary Reviews: Water*, 6, e1337, 2019.
- 560 Conti, S.: Artificial intelligence for weather forecasting, *Nature Reviews Electrical Engineering*, 1, 8–8, 2024.
- Cui, Y., Liu, F., Masouros, C., Xu, J., Han, T. X., and Eldar, Y. C.: Integrated sensing and communications: Background and applications, in: *Integrated Sensing and Communications*, pp. 3–21, Springer, 2023.
- David, N., Sendik, O., Messer, H., and Alpert, P.: Cellular network infrastructure-the future of fog monitoring?, *Bulletin of the American Meteorological Society*, 2014.
- 565 de Vos, L. W., Leijnse, H., Overeem, A., and Uijlenhoet, R.: Quality control for crowdsourced personal weather stations to enable operational rainfall monitoring, *Geophysical Research Letters*, 46, 8820–8829, 2019.
- Dong, F., Liu, F., Cui, Y., Wang, W., Han, K., and Wang, Z.: Sensing as a service in 6G perceptive networks: A unified framework for ISAC resource allocation, *IEEE Transactions on Wireless Communications*, 2022.
- El Hachem, A., Seidel, J., O’Hara, T., Villalobos Herrera, R., Overeem, A., Uijlenhoet, R., Bárdossy, A., and de Vos, L.: Overview and comparison of three quality control algorithms for rainfall data from personal weather stations, *Hydrology and Earth System Sciences Discussions*, 2023, 1–22, 2023.
- 570 El Hachem, A., Seidel, J., O’hara, T., Villalobos Herrera, R., Overeem, A., Uijlenhoet, R., Bárdossy, A., and De Vos, L.: A guide to using three open-source quality control algorithms for rainfall data from personal weather stations, *Hydrology and Earth System Sciences*, 28, 4715–4731, 2024.
- 575 Fencl, M., Nebuloni, R., Andersson, J. C., Bares, V., Blettner, N., Cazzaniga, G., Chwala, C., Colli, M., de Vos, L., El Hachem, A., et al.: Data formats and standards for opportunistic rainfall sensors, *Open Research Europe*, 3, 2023.



- Fencl, M., Bareš, V., Ostrometzky, J., Messer, H., Winterrath, T., Priestley, A., and Chwala, C.: A new initiative to facilitate the global collection of microwave link data and its use in hydrometeorology, *Bulletin of the American Meteorological Society*, 2025.
- 580 Fierz, C., Armstrong, R. L., Durand, Y., Etchevers, P., Greene, E., McClung, D. M., Nishimura, K., Satyawali, P. K., and Sokratov, S. A.:  
The International Classification for Seasonal Snow on the Ground, Tech. rep., IHP-VII Technical Documents in Hydrology N°83, IACS  
Contribution N°1, UNESCO-IHP, Paris, 2009.
- Graf, M., Chwala, C., Polz, J., and Kunstmann, H.: Rainfall estimation from a German-wide commercial microwave link network: optimized processing and validation for 1 year of data, *Hydrology and Earth System Sciences*, 24, 2931–2950, 2020.
- Habi, H. V. and Messer, H.: Wet-Dry Classification Using LSTM and Commercial Microwave Links, In Proc. of IEEE 10th Sensor Array  
585 and Multichannel Signal Processing Workshop (SAM), pp. 149–153, 2018.
- Hu, Q., Li, Z., Wang, L., Huang, Y., Wang, Y., and Li, L.: Rainfall spatial estimations: A review from spatial interpolation to multi-source data merging, *Water*, 11, 579, 2019.
- ITU-R P.530: Propagation data and prediction methods required for the design of terrestrial line-of-sight systems, ITU, 530-17, 2017.
- ITU-R P.838: Specific Attenuation Model for Rain for use in Prediction Methods, ITU, 838-3, 1992-1999-2003-2005, 2005.
- 590 Jacoby, D., Yu, S., Ostrometzky, J., Kadota, I., Zussman, G., and Messer, H.: OpenMesh Dataset – Wireless Signal Dataset for Opportunistic  
Urban Weather Sensing in New York City, <https://doi.org/10.5281/zenodo.15268340>, 2025.
- Janco, R., Ostrometzky, J., and Messer, H.: In-City Rain Mapping from Commercial Microwave Links—Challenges and Opportunities, *Sensors*, 23, 4653, 2023.
- Kaushik, A., Singh, R., Dayarathna, S., Senanayake, R., Di Renzo, M., Dajer, M., Ji, H., Kim, Y., Sciancalepore, V., Zappone, A., et al.:  
595 Toward Integrated Sensing and Communications for 6G: Key Enabling Technologies, Standardization, and Challenges, *IEEE Communi-  
cations Standards Magazine*, 8, 52–59, 2024.
- Kittivorawong, C., Theeranantachai, S., Tieanklin, N., Jang, E. H. B., and Heimerl, K.: Community Cellular Networks Coverage Visualizer, arXiv preprint arXiv:2408.00999, 2024.
- Kozak, R., Khorsand, K., Zarifi, T., Golovin, K., and Zarifi, M. H.: Patch antenna sensor for wireless ice and frost detection, *Scientific  
600 Reports*, 11, 13 707, 2021.
- Lompi, M., Tamagnone, P., Pacetti, T., Morbidelli, R., and Caporali, E.: Impacts of Rainfall Data Aggregation Time on Pluvial Flood Hazard in Urban Watersheds, *Water*, 14, 544, 2022.
- Mätzler, C.: Applications of the interaction of microwaves with the natural snow cover, *Remote sensing reviews*, 2, 259–387, 1987.
- Mesh, N.: NYC Mesh – Official Website, <https://www.nycmesh.net/>, 2025.
- 605 Messer, H. and Gazit, L.: From cellular networks to the garden hose: Advances in rainfall monitoring via cellular power measurements, in:  
2016 IEEE Global Conference on Signal and Information Processing (GlobalSIP), pp. 1012–1016, IEEE, 2016.
- Messer, H., Zinevich, A., and Alpert, P.: Environmental monitoring by wireless communication networks, *Science*, 312, 713–713, 2006.
- Messer, H., Zinevich, A., and Alpert, P.: Environmental sensor networks using existing wireless communication systems for rainfall and wind velocity measurements, *IEEE Instrumentation & Measurement Magazine*, 15, 32–38, 2012.
- 610 Niu, Y., Li, Y., Jin, D., Su, L., and Vasilakos, A. V.: A survey of millimeter wave communications (mmWave) for 5G: opportunities and challenges, *Wireless networks*, 21, 2657–2676, 2015.
- Olsen, R., Rogers, D., and Hodge, D.: The  $aR^b$  relation in the calculation of rain attenuation., *IEEE Trans. on Antennas and Propagation*, 26, 318–329, 1978.



- Ostrometzky, J.: Statistical signal processing of extreme attenuation measurements taken by commercial microwave links for rain monitoring, 615 Tel Aviv University, 2017.
- Ostrometzky, J. and Messer, H.: Opportunistic Weather Sensing by Smart City Wireless Communication Networks, *Sensors*, 24, 7901, 2024.
- Ostrometzky, J., Raich, R., Bao, L., Hansryd, J., and Messer, H.: The wet-antenna effect—A factor to be considered in future communication networks, *IEEE Transactions on Antennas and Propagation*, 66, 315–322, 2017.
- Overeem, A.: Commercial microwave link data for rainfall monitoring, 2023.
- 620 Overeem, A., Leijnse, H., and Uijlenhoet, R.: Measuring urban rainfall using microwave links from commercial cellular communication networks, *Water Resources Research*, 47, 2011.
- Ravuri, S., Lenc, K., Willson, M., Kangin, D., Lam, R., Mirowski, P., Fitzsimons, M., Athanassiadou, M., Kashem, S., Madge, S., et al.: Skilful precipitation nowcasting using deep generative models of radar, *Nature*, 597, 672–677, 2021.
- Rubin, Y., Rostkier-Edelstein, D., Chwala, C., and Alpert, P.: Challenges in diurnal humidity analysis from cellular microwave links (CML) 625 over Germany, *Remote Sensing*, 14, 2353, 2022.
- Samad, M. A., Diba, F. D., and Choi, D.-Y.: A survey of rain attenuation prediction models for terrestrial links—Current research challenges and state-of-the-art, *Sensors*, 21, 1207, 2021.
- Santos, P. M. e. a.: PortoLivingLab: An IoT-Based Sensing Platform for Smart Cities, *IEEE Internet of Things Journal*, 5, 523–532, <https://doi.org/10.1109/JIOT.2018.2791522>, 2018.
- 630 Schleiss, M. and Berne, A.: Identification of dry and rainy periods using telecommunication microwave links, *IEEE Geoscience and Remote Sensing Letters*, 7, 611–615, 2010.
- Schleiss, M., Rieckermann, J., and Berne, A.: Quantification and modeling of wet-antenna attenuation for commercial microwave links, *IEEE Geoscience and Remote Sensing Letters*, 10, 1195–1199, 2013.
- Seker, C., Güneser, M. T., and Ozturk, T.: A Review of Millimeter Wave Communication for 5G, in: *Proc. 2nd Int. Symp. on Multidisciplinary Studies and Innovative Technologies (ISMSIT)*, pp. 1–5, IEEE, 2018.
- 635 Špačková, A., Bareš, V., Fencl, M., Schleiss, M., Jaffrain, J., Berne, A., and Rieckermann, J.: A year of attenuation data from a commercial dual-polarized duplex microwave link with concurrent disdrometer, rain gauge, and weather observations, *Earth System Science Data*, 13, 4219–4240, 2021.
- Upton, G., Holt, A., Cummings, R., Rahimi, A., and Goddard, J.: Microwave links: The future for urban rainfall measurement?, *Atmospheric research*, 77, 300–312, 2005.
- 640 WMO, W.: Guide to instruments and methods of observation, World Meteorological Organization WMO, URL <https://library.wmo.int/index.php>, 2018.
- Xu, J., Lyu, Z., Song, X., Liu, F., Cui, Y., Masouros, C., Han, T. X., Eldar, Y. C., and Cui, S.: ISAC with Emerging Communication Technologies, in: *Integrated Sensing and Comm.*, pp. 589–619, Springer, 2023.
- 645 Zawadzki, I.: Factors affecting the precision of radar measurements of rain., in: *22nd conference on radar meteorology*, Zurich, Switzerland, pp. 251–256, 1984.
- Zhang, P., Liu, X., and Pu, K.: Precipitation monitoring using commercial microwave links: current status, challenges and prospectives, *Remote Sensing*, 15, 4821, 2023.
- Zhang, Q. S.: Environment pollution analysis on smart cities using wireless sensor networks, *Strategic Planning for Energy and the Environ-* 650 *ment*, pp. 239–262, 2023.